

Heavy Quarkonium Spectrum and Decay Constants from a Neural-Network-Based Holographic Model

Yu Zhang,^{1,2} Xun Chen,^{1,2,3,*} and Miguel Angel Martin Contreras^{1,2,†}

¹*School of Nuclear Science and Technology,*

University of South China Hengyang, No 28,

West Changsheng Road, Hengyang City, Hunan Province, China.

²*Key Laboratory of Advanced Nuclear Energy Design and Safety,*

Ministry of Education, Hengyang, 421001, China

³*INFN — Istituto Nazionale di Fisica Nucleare —*

Sezione di Bari Via Orabona 4, 70125, Bari, Italy

(Dated: January 27, 2026)

Abstract

We present a data-driven inverse construction of the dilaton field in a bottom-up AdS/QCD description of heavy vector quarkonia. Instead of adopting an *ad hoc* analytic ansatz, we use a multilayer perceptron to learn $\Phi'(z)$ as a smooth function of the holographic coordinate, with $\Phi(0) = 0$ imposed to ensure ultraviolet consistency. The dilaton and its derivatives obtained by automatic differentiation generate the holographic potential $U(z)$, and the associated Schrödinger-like equation is discretized and diagonalized to extract the low-lying eigenmodes. Masses and decay constants are then evaluated from the eigenvalues and the near-boundary behavior of the bulk-to-boundary modes. Training on PDG data for charmonium and bottomonium yields a non-quadratic dilaton profile that resolves the longstanding difficulty of simultaneously reproducing both the heavy-quarkonium spectrum and the monotonic suppression of leptonic decay constants with radial excitation. The combined fit achieves RMS deviations of 1.26% (charmonium) and 3.32% (bottomonium). This work establishes neural-network reconstruction as a flexible tool for holographic modeling and provides a basis for future extensions incorporating additional channels, lattice constraints, or finite-temperature backgrounds.

* chenxun@usc.edu.cn

† miguelangel.martin@usc.edu.cn

I. INTRODUCTION

Quantum Chromodynamics (QCD) is the fundamental theory that describes the strong interaction. However, in the low-energy and strongly coupled regime, analytical solutions to QCD become extremely difficult to obtain, and traditional perturbative methods are no longer effective. This limitation has motivated the development of various non-perturbative approaches, among which the AdS/QCD model [1–4] based on the holographic principle has attracted considerable attention in recent years. The idea of AdS/QCD originates from the AdS/CFT correspondence, which reveals a profound connection between strongly coupled gauge theories and weakly coupled gravity theories [5–7]. Depending on the construction scheme, AdS/QCD models can be classified into top-down and bottom-up approaches: the former are derived from string theory, where probe branes are introduced into the bulk geometry to set the energy scale and break conformal symmetry [8–10]; the latter directly implement deformations in the five-dimensional spacetime to reproduce hadronic properties observed in experiments. Within the bottom-up framework, the hard-wall [1, 2, 11] and soft-wall [12] models are the most widely used. In particular, the soft-wall model is well-suited for studying meson radial excitations, as it naturally reproduces the linear Regge trajectories of hadron masses. These models have been extensively applied to the study of meson spectroscopy [12–21] and heavy quarkonia [22–25]. The latter have introduced quadratic-like dilaton fields to fit heavy vector quarkonia with linear radial Regge trajectories.

However, for heavy quarkonium systems, the radial Regge trajectory hypothesis breaks down, according to Bethe-Salpeter Theory [26–28], implying Regge trajectories can be parametrized as $M_n^2 = a(n + b)^\nu$. This non-linearity, at the holographic level, can be translated into the dilaton field $\Phi(z)$ if a non-quadratic version is considered, as it was introduced in [29]. Recently, this dilaton phenomenological *ansatz* was derived from WKB analysis [30].

On the purely phenomenological side, heavy quarkonia, including charmonium ($c\bar{c}$) and bottomonium ($b\bar{b}$), play a central role in hadron physics due to their large quark masses, which simplify their internal dynamics. These systems provide an effective framework for investigating the non-perturbative regime of QCD. Heavy quarkonia connect perturbative calculations with strong-coupling phenomena, enabling rigorous tests of fundamental QCD concepts such as confinement and mass generation. Systematic analyses of their mass spectra and decay constants yield valuable information about the quark-antiquark potential.

Furthermore, the well-characterized properties of heavy quarkonia serve as essential benchmarks for theoretical models, including lattice QCD and holographic methods, that seek to describe the strong interaction. Experimentally, the decay constants of charmonium and bottomonium can be extracted from the heavy vector to dileptons ($V \rightarrow l\bar{l}$) decay width. These constants display a monotonic decrease with increasing excitation level [31].

This trend indicates that higher excited states are progressively less stable [32, 33], a defining feature of heavy quarkonium spectroscopy. In contrast, the decay constants of light mesons, such as the ρ , ϕ , and ω mesons, are only known experimentally for their ground states [31]. However, from theoretical approaches such as Relativistic Hamiltonian Dynamics [34], Light-Front Dynamics [35, 36], or the Nambu-Jona-Lasinio Model [37], one can infer the decay constants of excited states. These theoretical estimates seem to show a decrease in decay constants with increasing radial excitation level, suggesting that this pattern may be universal in meson spectroscopy. It should be emphasized that, for heavy-light mesons such as D and B, the decay constants are extracted from electroweak processes rather than electromagnetic ones. Consequently, the underlying mechanism differs from that of heavy quarkonia, where decay constants are obtained from electromagnetic decays into dileptons.

However, the existing holographic models still have limitations in describing heavy quarkonium spectroscopy, as they cannot simultaneously reproduce both the mass spectrum and the decay constants with high accuracy. For example, Ref. [23] improved the masses and decay constants of J/ψ and ψ' by modifying the holographic potential, but failed to reproduce the experimental observation that the decay constants decrease with increasing excitation level. Refs. [25, 38–40] introduced a finite z_{uv} cutoff in the AdS slice to set the ultraviolet scale, which led to a decreasing trend of decay constants with higher excitation levels. However, the slope of this decrease was much smaller than that observed in the experimental results, providing only qualitative agreement. Another class of holographic models proposed in Ref. [41] successfully addressed the *slope problem* of the decay constants and accurately reproduced the spectra of charmonium and bottomonium decay constants. However, they could not simultaneously provide a precise description of the mass spectrum. In Refs. [42, 43], the authors inferred the role played by the ultraviolet (UV) limit of the dilaton field $\Phi(z)$ in determining decay constants. Therefore, modifying this limit allows us to induce the expected decrease in decay constants. Thus, transformations like *isospectrality* [44] or geometric deformations (as UV cutoffs) also modify decay constants.

Recently, machine learning techniques, particularly multilayer perceptrons (MLPs), have shown significant promise in addressing complex scientific challenges [45–55]. The universal approximation theorem [56] establishes that an MLP can approximate any continuous function, provided a sufficient number of hidden neurons are present. This capability renders MLPs highly effective for solving partial differential equations [57–60] and modeling inverse problems. Compared to traditional polynomial fitting or parametrization approaches, MLPs offer greater expressive power and enhance predictive accuracy while maintaining physical constraints.

To the best of our knowledge, this work represents the first application of MLPs to reconstruct the dilaton field directly $\Phi(z)$ within a bottom-up AdS/QCD model. Unlike previous approaches that rely on *ad hoc* parametrizations, our method uses experimental data on heavy quarkonium masses and decay constants to determine $\Phi(z)$ in a data-driven manner. This allows for a unified and highly accurate description of both spectroscopic and decay properties, addressing a longstanding challenge in holographic QCD.

In recent years, the rapid advancement of machine learning techniques [61–70] has facilitated the introduction of deep learning into the study of holographic QCD, offering novel perspectives for model construction [71–81]. In contrast to traditional bottom-up models that depend on *ad hoc* specified potentials or dilaton profiles, data-driven approaches leverage experimental or lattice QCD data to determine model parameters, thereby enhancing both reliability and interpretability. Recent studies demonstrate that holographic models integrated with neural networks can effectively address inverse problems and achieve superior performance in the non-perturbative regime of the strong interaction [71, 72, 77]. In this manuscript, deep learning techniques were employed to reconstruct the dilaton field using a MLP. This approach enabled a unified, precise description of the mass spectra and decay constants of the radial excitations of charmonium and bottomonium. The model predictions show excellent agreement with experimental data, with root-mean-square errors of approximately 1.26% for charmonium and 3.32% for bottomonium, thereby providing an effective tool for investigating heavy-quarkonium spectroscopy at zero temperature.

The structure of this paper is as follows. Section II introduces the motivation and construction of the holographic model, with particular emphasis on reconstructing the dilaton field using a MPL. Section III presents the spectroscopy of charmonium and bottomonium at zero temperature, including both mass spectra and decay constants, and systematically

compares predictions with experimental data to assess the model validity. Section IV summarizes the main results and innovations of this work and discusses potential applications of the model in future studies of heavy quarkonia.

II. HOLOGRAPHIC MODEL

Reference [43] proposed a forward-direction construction within the bottom-up AdS/QCD framework, introducing an appropriate dilaton profile to simultaneously describe the mass spectra and decay constants of heavy quarkonia. Although the model is phenomenological, it demonstrates strong agreement with experimental data. This approach has also been applied and refined in various holographic models to investigate the spectral properties of heavy quarkonia at finite temperature. Building on this forward framework, the corresponding vector-field action and equations of motion are presented below as the foundation for the subsequent inverse analysis.

At zero temperature, the background geometry is taken to be the five-dimensional anti-de Sitter (AdS₅) spacetime, whose metric in the Poincaré patch is

$$ds^2 = \frac{R^2}{z^2} (\eta_{\mu\nu} dx^\mu dx^\nu - dz^2), \quad (1)$$

where z is the holographic coordinate, with $z \rightarrow 0$ corresponding to the ultraviolet (UV) boundary and $z \rightarrow \infty$ to the infrared (IR) region. Here $\eta_{\mu\nu} = \text{diag}(1, -1, -1, -1)$ is the four-dimensional Minkowski metric, and R is the AdS radius.

The action for the gauge field is written as

$$S_{\text{Vector } Q\bar{Q}} = -\frac{1}{4g_5^2} \int d^5x \sqrt{-g} e^{-\Phi(z)} g^{mp} g^{nr} F_{mn} F_{pr}, \quad (2)$$

where $F_{mn} = \partial_m V_n - \partial_n V_m$ is the field strength tensor of the five-dimensional gauge field V_m ; g denotes the determinant of the five-dimensional metric; g^{mp} and g^{nr} are the inverse metric components used to raise covariant indices to contravariant ones and perform contractions; and $\Phi(z)$ is the dilaton field, whose exponential factor $e^{-\Phi(z)}$ encodes the nonperturbative effects of QCD.

By varying the action with respect to V_m , the equation of motion is obtained as

$$\partial_m (\sqrt{-g} e^{-\Phi(z)} g^{np} g^{mr} F_{pr}) = 0, \quad (3)$$

where $F_{mn} \equiv \partial_m V_n - \partial_n V_m$.

In the bottom-up AdS/QCD framework, heavy vector quarkonia can be described by a five-dimensional Abelian massless gauge field. This setting follows from the standard field-operator correspondence [6], where the bulk mass is related to the scaling dimension Δ of the boundary operator creating hadrons by

$$M_5^2 R^2 = (\Delta - 1)(\Delta - 3), \quad (4)$$

and for the vector current $\bar{Q}\gamma_\mu Q$ operator with $\Delta = 3$, one obtains

$$M_5^2 R^2 = 0. \quad (5)$$

In the axial gauge $V_z = 0$ and with the transverse condition $\partial^\mu V_\mu = 0$, we take the plane-wave ansatz

$$V_\mu(x, z) = \epsilon_\mu v(z) e^{ip \cdot x}, \quad (6)$$

where ϵ_μ is the polarization vector and $p^2 = m_n^2$ is the on-shell mass condition for vector mesons. Substituting this ansatz into the equation of motion leads to the *Sturm-Liouville* equation for the vector bulk modes

$$\partial_z (e^{-B(z)} \partial_z v_n(z)) + m_n^2 e^{-B(z)} v_n(z) = 0, \quad (7)$$

where the *background function* $B(z)$ is defined as

$$B(z) = \Phi(z) - \log \left(\frac{R}{z} \right). \quad (8)$$

One of the main consequences of confinement is the emergence of bound states of quarks, i.e., hadrons. At the holographic level, confinement is achieved by breaking bulk conformal invariance. To do so, it is customary to use a hard cutoff in AdS space [3, 82] (hard-wall model) or a dilaton field $\Phi(z)$, static [12] or dynamically [83] generated soft-wall model. Analogously to quantum mechanics, the hard-wall model is like solving the square-well potential, and the soft-wall model is like solving a 2-dimensional harmonic oscillator. It is in this context that *in bottom-up models, confinement is realized with the emergence of bound states in the AdS bulk, dual to hadrons at the boundary*.

In the particular case of the soft-wall model, the dilaton is defined by a static quadratic form $\Phi(z) = \kappa^2 z^2$, with κ the energy scale that sets hadron masses. The emerging radial Regge trajectories M_n^2 are linear, and the decay constant spectrum f_n is degenerate:

$$M_n^2 = 4\kappa^2(n+1), \quad (9)$$

$$f_n^2 = \frac{2\kappa^2}{g_5^2}, \quad (10)$$

where n is the radial excitation number.

However, the linearity observed in the mass spectrum does not satisfy the phenomenological constraints imposed by the Bethe-Salpeter theory [26], since the heavy quark mass becomes relevant in this case. On the pure phenomenological side, from non-relativistic QCD, the one-gluon exchange term, which is Coulomb-like, has a stronger *inertial* effect on the heavy meson ground state than the linear confinement term [84]. Thus, for heavy vector mesons, a *non-quadratic dilaton is expected* [30]. When high radial excitations are considered, the confinement term in the Cornell potential becomes relevant, implying that linearity can be recovered. However, the existing heavy spectra do not extend beyond $n = 6$, as in the case of bottomonium, or $n = 4$, for charmonium. Therefore, it is consistent to expect a non-linear parametrization for Regge trajectories.

Regarding the decay constants for vector mesons, neither the hard-wall nor the soft-wall model describes them properly. In the former case, decay constants increase with radial excitations [85]. In the latter, the decay constants are degenerate. Although this outcome may seem counterintuitive, in the context of large- N_c QCD, it is expected. At large Q^2 , the asymptotics of the vector meson correlation functions are given by [86, 87]

$$\Pi(Q^2) \sim \frac{N_c}{12\pi^2} \left[\ln \left(\frac{Q^2}{m_Q^2} \right) - \frac{6m_Q^2}{Q^2} + \mathcal{O} \left(\frac{m_Q^4}{Q^4} \right) \right] \sim \sum_n \frac{f_n^2}{Q^2 - M_n^2} \quad (11)$$

When the sum is approximated using the Euler-Maclaurin summation formula [88], the decay constants, as residues of $\Pi(q^2)$, can be written as

$$f_n^2 \propto \frac{dM_n^2}{dn} \propto \text{constant}, \quad (12)$$

which holds at least for $n \rightarrow \infty$ and linear M_n^2 . This picture is consistent with the *string picture of mesons*. Notice that, since the meson size is given by the string length $l \sim M_n$,

for the leptonic decay width one gets $\Gamma_{V_n \rightarrow e^+ e^-} \sim 1/l \sim 1/M_n$. However, on the other hand, $\Gamma_{V_n \rightarrow e^+ e^-} \sim f_n^2/M_n$. Thus, $f_n \sim \text{constant}$, in agreement with the soft-wall holographic counterpart.

Nevertheless, this particular scaling behavior is expected for light mesons, for which the relativistic string picture applies. In the heavy case, the non-relativistic kinematics, the mass dominance $M_n \sim 2m_Q$, different size scaling (heavy mesons do not scale linearly with the mass), and the wave-function suppression at the origin (as described by the Van Royen–Weisskopf formula), break this ideal picture [89].

Therefore, this phenomenological analysis motivates moving beyond the quadratic static dilaton ansatz to describe both the electromagnetic decay constants and the radial Regge trajectories of heavy vector mesons.

In this work, we do not assume an explicit analytic form for $\Phi(z)$; instead, we determine it through an inverse method based on experimental data, ensuring that the resulting $\Phi(z)$ satisfies both IR and UV constraints for the potential defined as

$$U(z)|_{z \rightarrow 0} = \frac{A}{z^2} \quad (13)$$

$$U(z)|_{z \rightarrow \infty} = B z^2 + f(z) \quad (14)$$

where the condition (13) corresponds to the UV constraint, defined by the field/operator itself, since the parameter A carries the information about the conformal dimension Δ . In bottom-up models, this parameter is fixed to be $3/4$ for vector states. The second condition (14) controls variations from the standard quadratic dilaton form observed in the Soft-wall model. Any non-linearities expected in the spectrum will be encoded in the function $f(z)$. These conditions provide a suitable background for subsequent calculations of the mass spectrum and decay constants.

By redefining the bulk field with the *Bogoliubov transformation* as $v_n(z) = e^{B(z)/2} \psi_n(z)$ using the background function, the Sturm-Liouville equation (7) can be cast into a *Schrödinger-like* form

$$-\psi_n''(z) + U(z) \psi(z) = m_n^2 \psi(z), \quad (15)$$

where the holographic bottom-up confining potential for vector mesons is written as:

$$U(z) = \frac{1}{4}B'(z)^2 - \frac{1}{2}B''(z). \quad (16)$$

For numerical implementation, the effective potential function $U(z)$ is directly expanded in terms of the derivatives of the dilaton field $\Phi(z)$ as follows:

$$U(z) = \frac{3}{4z^2} + \frac{\Phi'(z)}{2z} + \frac{\Phi'(z)^2}{4} - \frac{\Phi''(z)}{2} \quad (17)$$

In the framework of holographic QCD, the decay constant f_n of a vector meson is determined by the behavior of the five-dimensional gauge field near the UV boundary. For the n -th eigenstate, with mass denoted by M_n and radial wave-function $v_n(z)$, one has

$$f_n = \frac{1}{g_5 M_n} \lim_{z \rightarrow 0} [e^{-B(z)} \partial_z v_n(z)], \quad (18)$$

where g_5 is the five-dimensional gauge coupling constant and $B(z)$ is the background function defined earlier. The limit $z \rightarrow 0$ corresponds to the UV boundary of the AdS space, where the five-dimensional field is matched to the external source of QCD in four dimensions, thereby relating the boundary current to the four-dimensional vector current matrix element by the holographic dictionary.

III. MODELING HOLOGRAPHIC QCD WITH MLP

Based on the MLPs, we reconstruct the dilaton field $\Phi(z)$ within the AdS/QCD framework. The background profile is directly inferred from experimental data, specifically the mass spectrum and decay constants of charmonium and bottomonium states. The architecture of the neural network is illustrated in Fig. 1, consisting of five hidden layers with 128 neurons each. Trainable parameters include the weights and biases of all hidden layers, denoted as $w_n^{(1)}, w_n^{(2)}, \dots, w_n^{(5)}$, as well as the output layer parameters v_n , all optimized using the Adam gradient descent algorithm. The training objective is to minimize the mean squared error between the predicted mass spectrum and the experimental data. To provide a unified quantitative measure of the overall fitting accuracy, we introduce the root-mean-square (RMS) deviation, defined as

$$\text{RMS} = \sqrt{\frac{1}{N} \sum_{i=1}^N \left(\frac{\mathcal{O}_i^{\text{pre}} - \mathcal{O}_i^{\text{exp}}}{\mathcal{O}_i^{\text{exp}}} \right)^2} \times 100\%, \quad (19)$$

where N denotes the total number of observables, including both masses and decay constants, and $\mathcal{O}_i^{\text{pre}}$ and $\mathcal{O}_i^{\text{exp}}$ represent the predicted and experimental values of the i -th observable, respectively. This definition provides a single indicator that simultaneously reflects the model performance across both spectroscopic and dynamical quantities, offering a clear, intuitive measure of overall agreement with experimental data.

The key idea is as follows: the function $\Phi'(z)$ is represented by a deep neural network that takes the holographic coordinate z as input. During training, the network outputs $\Phi'(z)$, and its exact derivative $d\Phi'(z)/dz$ is computed by automatic differentiation. These quantities are combined according to Eq. (17) to reconstruct the potential $U(z)$. The loss function, defined as the **SmoothL1Loss** between this reconstructed potential and the target potential from a pre-trained model, is minimized using the *Adam optimizer* with a cosine-annealing learning rate schedule. Training converges within 10^4 iterations, with automatic gradient clipping preventing instability. The entire procedure operates in a mesh-free manner without explicit discretization or Hamiltonian matrix construction.

A \tanh activation function follows each hidden layer, while the output layer uses no activation. To enforce ultraviolet (UV) boundary regularity, the network output is structurally transformed to satisfy the condition $\Phi(0) = 0$, thereby ensuring consistency with the theoretical requirements of the AdS/QCD model.

Once the dilaton field is obtained, its first and second derivatives are computed by automatic differentiation and substituted into Eq. (17) to construct the effective potential $U(z)$. The Schrödinger-like equation, Eq. (15), is discretized on a finite grid and solved by Hamiltonian diagonalization to extract the mass eigenvalues m_n and corresponding wave functions $\psi_n(z)$. The decay constants f_n are computed using Eq. (18), which depends on the near-boundary behavior of both $\Phi(z)$ and $\psi_n(z)$.

The reconstructed dilaton field exhibits a non-quadratic expansion near the UV boundary, while its rapid growth in the IR reflects the confining nature of QCD. This non-quadratic IR behavior is crucial for reproducing the non-linear Regge trajectories and decreasing decay constants observed in heavy quarkonia. The deviation from a purely quadratic form underscores the importance of heavy-quark mass effects, which break the relativistic string picture applicable to light mesons.

In the final implementation, we adopted a more rigorous training strategy. Instead of directly fitting the effective potential $U(z)$, we employed a neural network to reconstruct the

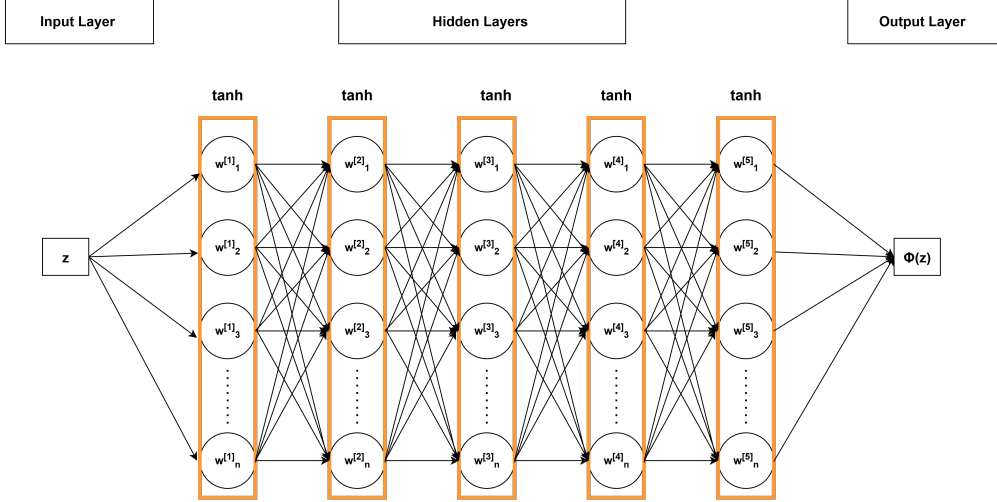


FIG. 1: A neural network flowchart for reconstructing the dilaton field $\Phi(z)$.

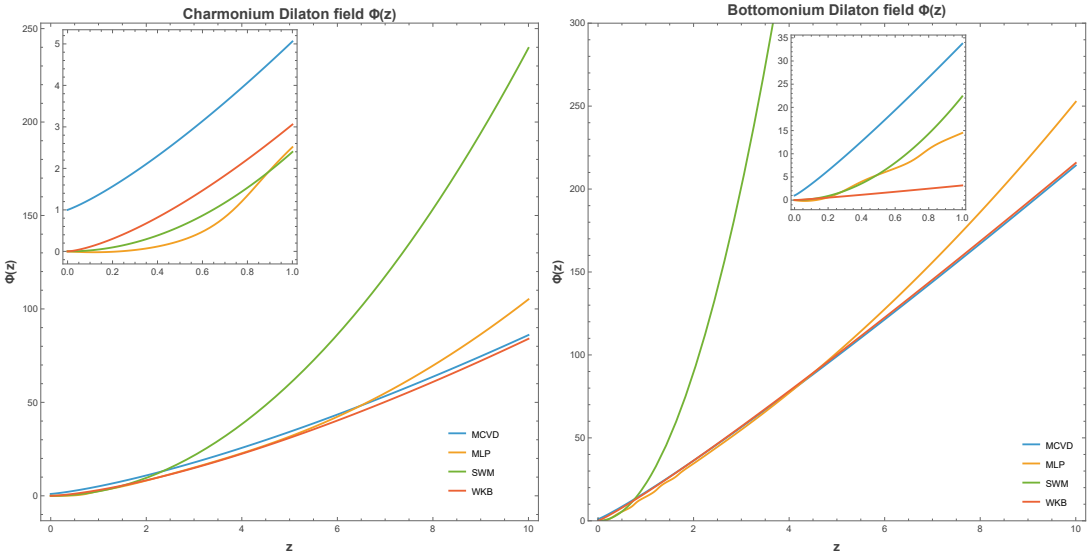


FIG. 2: Dilaton fields $\Phi(z)$ for charmonium (left) and bottomonium (right) obtained from different approaches: Non-linear approach MCVD [43] (blue), Machine Learning Perceptron (MLP) in orange, soft-Wall model [12], and WKB approach [44].

dilaton field $\Phi(z)$, with the ultraviolet boundary condition $\Phi(0) = 0$ explicitly imposed to ensure compatibility with the AdS/QCD framework. Once the dilaton profile was obtained, the effective potential $U(z)$ was analytically derived from $\Phi(z)$ and its first and second derivatives. This procedure guarantees that the definition of the potential strictly follows the holographic construction, while avoiding the introduction of an *ad hoc* base-plus-correction structure. As a result, the model successfully reproduces the decreasing trend of decay

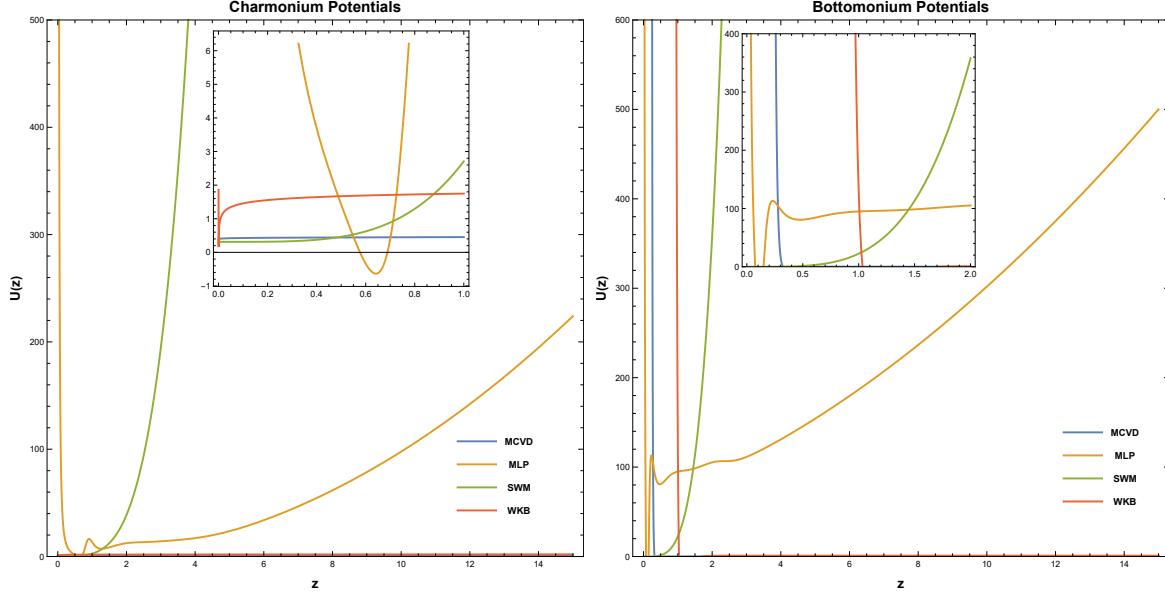


FIG. 3: Potentials $U(z)$ for charmonium (left) and bottomonium (right) obtained from different approaches: Non-linear approach MCVD [43] (blue), Machine Learning Perceptron (MLP) in orange, soft-wall model [12], and WKB approach [44].

constants and predicts the masses of higher excited states.

After the training converges, the reconstructed dilaton field is shown in Fig. 2. In the UV region, $\Phi(z)$ exhibits an approximate non-quadratic expansion, different from the expected quadratic one, characteristic of the soft-wall model, lifting the degeneracy of the decay constants. In contrast, in the IR region, it grows rapidly, reflecting the confinement effect. These corrections are essential for reproducing the experimental spectrum. Compared to the conventional analytical soft-wall ansatz, our data-driven reconstruction yields an IR growth that is more consistent with experimental requirements, thereby improving the description of higher excited states.

To further highlight the advantages of this work, Fig. 2 presents a comparison of the MLP reconstruction results with three existing models: the traditional soft-wall model, the WKB analysis, and the results for a non-quadratic dilaton [90], which we call MCVD (Martin-Contreras, Vega, and Diles). It can be seen that the soft-wall model exhibits large deviations in the masses and decay constants of highly excited states; the WKB method, although improving the overall trend, still shows significant discrepancies in the infrared behavior of the dilaton compared with other static dilatons (see Fig. 2). The model of [90] achieves partial success in reproducing the decreasing trend of decay constants, but its description of

Charmonium States $I^G(J^{PC}) = 0^+(1^{--})$							
n	State	M_{Exp} (MeV)	M_{MLP} (MeV)	$\%M$	f_{Exp} (MeV)	f_{MLP} (MeV)	$\%f$
1	J/ψ	3096.900 ± 0.006	3097.2	0.01	416.16 ± 5.25	416.2	0.01
2	$\psi(2S)$	3686.097 ± 0.010	3686.5	0.01	296.08 ± 2.51	296.1	0.01
3	$\psi(4040)$	4040 ± 4	4040.4	0.01	187.13 ± 7.61	186.9	0.1
4	$\psi(4415)$	4415 ± 5	4416.52	0.03	160.78 ± 9.70	157.63	2.0

TABLE I: Summary of results for charmonium states. Theoretical predictions based on neural network reconstruction results are listed in the M_{MLP} and f_{MLP} columns. The corresponding relative errors are shown in the $\%M$ and $\%f$ columns. Experimental data are taken from PDG [91] and the total root-mean-square (RMS) error is $\delta_{\text{RMS}} = 1.26\%$.

Bottomonium States $I^G(J^{PC}) = 0^+(1^{--})$							
n	State	M_{Exp} (MeV)	M_{MLP} (MeV)	$\%M$	f_{Exp} (MeV)	f_{MLP} (MeV)	$\%f$
1	$\Upsilon(1S)$	9460.4 ± 0.1	9460.42	0.0002	714.99 ± 2.40	715.1	0.01
2	$\Upsilon(2S)$	10023.4 ± 0.5	10023.42	0.0002	497.37 ± 2.23	497.4	0.009
3	$\Upsilon(3S)$	10355.1 ± 0.5	10355.08	0.0002	430.11 ± 1.94	430.2	0.2
4	$\Upsilon(4S)$	10579.4 ± 1.2	10579.41	0.0001	340.65 ± 9.08	340.9	0.4
5	$\Upsilon(10860)$	$10885.2^{+2.6}_{-1.6}$	10863.27	0.2	310.91 ± 60.80	316.66	1.8
6	$\Upsilon(11020)$	11000 ± 4	11149.99	1.3	240.13 ± 27.70	267.33	11.3

TABLE II: Summary of results for bottomonium states. Theoretical predictions based on neural network reconstruction results are listed in the M_{MLP} and f_{MLP} columns. The corresponding relative errors are shown in the $\%M$ and $\%f$ columns. Experimental data are taken from PDG [91] and the total root-mean-square (RMS) error is $\delta_{\text{RMS}} = 3.32\%$.

the mass spectrum remains limited. In contrast, the MLP reconstruction results are overall more consistent with the experimental data, particularly in simultaneously reproducing both the mass spectrum and the decay constants with higher accuracy. This comparison further confirms the effectiveness of data-driven approaches in the study of nonperturbative QCD.

For completeness, Fig. 3 presents the effective potentials $U(z)$ reconstructed for charmonium and bottomonium. In the ultraviolet region, the potentials exhibit near-harmonic-oscillator behavior. In contrast, in the infrared, they develop nonlinear corrections that are

crucial for reproducing the experimental mass spectra and decay constants. The comparison highlights that the neural network reconstruction not only captures the dilaton profile but also provides a consistent effective potential, thereby reinforcing the reliability of the approach.

From Tables I and II, it is clear that the neural network demonstrates good fitting performance on the training dataset. The predicted mass spectrum and decay constants for the ground state and the first excited state are in excellent agreement with the experimental values, with relative errors remaining within acceptable ranges. As the excitation level increases, the deviations become larger, but the overall trend remains consistent with the experimental spectrum. These results indicate that the neural network not only satisfies the boundary condition $\Phi(0) = 0$, but also effectively captures the systematic behavior of the spectrum. The comparison in the tables further supports the model’s validity and verifies the neural network’s reliability in reconstructing the dilaton field.

IV. SUMMARY

In this study, we employ an MLP to reconstruct the dilaton field $\Phi(z)$ within the AdS/QCD framework directly from experimental data. The neural network is used to parameterize $\Phi'(z)$, and its derivative $\Phi''(z)$ is obtained by automatic differentiation. These quantities are combined according to Eq. (17) to construct the effective potential $U(z)$.

The Schrödinger-like equation is discretized on a finite grid using a second-order finite-difference scheme, and the corresponding Hamiltonian matrix is explicitly constructed and diagonalized to obtain the low-lying eigenvalues. The Adam optimizer is then used to minimize the discrepancy between the predicted spectrum and the experimental data, with the training converging typically within 10^4 iterations.

To verify the validity of the reconstruction, we apply the obtained dilaton profile to the calculation of the heavy-quark spectrum and compare the results with experimental data. The results show that MLPs are highly effective at solving inverse problems and provide accurate numerical solutions. This demonstrates that neural networks can serve as a reliable tool for data-driven holographic modeling.

The findings not only provide an effective paradigm for applying neural networks to holographic QCD but also point to new directions for subsequent research. These directions

include a more systematic exploration of the relation between the reconstructed background fields and different hadronic observables, as well as the integration of data-driven methods with analytical holographic models, aiming at a more comprehensive understanding of the nonperturbative dynamics of QCD.

It should be emphasized that the present results mainly focus on the zero-temperature spectrum. On the one hand, the framework can be naturally extended to finite-temperature backgrounds to investigate spectral functions and melting phenomena. On the other hand, this work may inspire future efforts to incorporate additional experimental inputs, such as meson spectra in other channels, decay widths, or the equation of state, into the holographic reconstruction. Ultimately, such developments may enable the construction of a unified data-driven holographic framework capable of describing broader aspects of strong-interaction physics.

While the model achieves excellent agreement with existing data, its predictive power for higher radial excitations ($n > 6$) remains untested due to limited experimental inputs. Furthermore, the current framework does not incorporate open-flavor thresholds or coupled-channel effects, which may influence higher-lying states. Future extensions could integrate lattice QCD data, finite-temperature backgrounds, or external magnetic fields to explore thermal spectral functions and magnetized quarkonia. Incorporating additional observables such as decay widths and form factors could further constrain the dilaton profile and enhance the universality of data-driven dilaton-based models.

ACKNOWLEDGEMENT

This work is supported by National Natural Science Foundation of China (NSFC) Grants No. 12405154 (X. Chen), 12350410371 (M.A. Martin Contreras), and the European Union – Next Generation EU through the research grant number P2022Z4P4B “SOPHYA - Sustainable Optimised PHYSics Algorithms: fundamental physics to build an advanced society” under the program PRIN 2022 PNRR of the Italian Ministero dell’Università e Ricerca (MUR).

REFERENCES

- [1] J. Polchinski and M. J. Strassler, *Phys. Rev. Lett.* **88**, 031601 (2002), arXiv:hep-th/0109174.
- [2] H. Boschi-Filho and N. R. F. Braga, *JHEP* **05**, 009 (2003), arXiv:hep-th/0212207.
- [3] J. Erlich, E. Katz, D. T. Son, and M. A. Stephanov, *Phys. Rev. Lett.* **95**, 261602 (2005), arXiv:hep-ph/0501128.
- [4] S. J. Brodsky and G. F. de Teramond, *Phys. Rev. D* **77**, 056007 (2008), arXiv:0707.3859 [hep-ph].
- [5] J. M. Maldacena, *Int. J. Theor. Phys.* **38**, 1113 (1999), arXiv:hep-th/9711200.
- [6] O. Aharony, S. S. Gubser, J. M. Maldacena, H. Ooguri, and Y. Oz, *Phys. Rept.* **323**, 183 (2000), arXiv:hep-th/9905111.
- [7] S. S. Gubser, I. R. Klebanov, and A. M. Polyakov, *Phys. Lett. B* **428**, 105 (1998), arXiv:hep-th/9802109.
- [8] A. Karch and E. Katz, *JHEP* **06**, 043 (2002), arXiv:hep-th/0205236.
- [9] T. Sakai and S. Sugimoto, *Prog. Theor. Phys.* **113**, 843 (2005), arXiv:hep-th/0412141.
- [10] T. Sakai and S. Sugimoto, *Prog. Theor. Phys.* **114**, 1083 (2005), arXiv:hep-th/0507073.
- [11] H. Boschi-Filho and N. R. F. Braga, *Eur. Phys. J. C* **32**, 529 (2004), arXiv:hep-th/0209080.
- [12] A. Karch, E. Katz, D. T. Son, and M. A. Stephanov, *Phys. Rev. D* **74**, 015005 (2006), arXiv:hep-ph/0602229 [hep-ph].
- [13] H. R. Grigoryan and A. V. Radyushkin, *Phys. Rev. D* **76**, 095007 (2007), arXiv:0706.1543 [hep-ph].
- [14] J. Erdmenger, N. Evans, I. Kirsch, and E. Threlfall, *Eur. Phys. J. A* **35**, 81 (2008), arXiv:0711.4467 [hep-th].
- [15] P. Colangelo, F. De Fazio, F. Giannuzzi, F. Jugeau, and S. Nicotri, *Phys. Rev. D* **78**, 055009 (2008), arXiv:0807.1054 [hep-ph].
- [16] A. Ballon Bayona, H. Boschi-Filho, N. R. F. Braga, and M. A. C. Torres, *JHEP* **01**, 052 (2010), arXiv:0911.0023 [hep-th].
- [17] A. L. Cotrone, A. Dymarsky, and S. Kuperstein, *JHEP* **03**, 005 (2011), arXiv:1010.1017 [hep-th].

- [18] D. Li and M. Huang, [JHEP **11**, 088 \(2013\)](#), arXiv:1303.6929 [hep-ph].
- [19] N. Wen, X. Cao, J. Chao, and H. Liu, [Phys. Rev. D **109**, 086021 \(2024\)](#), arXiv:2402.06239 [hep-th].
- [20] X. Cao, S. Qiu, H. Liu, and D. Li, [JHEP **08**, 005 \(2021\)](#), arXiv:2102.10946 [hep-ph].
- [21] M. Thomas Arun and R. Pal, (2025), arXiv:2512.16450 [hep-ph].
- [22] Y. Kim, J.-P. Lee, and S. H. Lee, [Phys. Rev. D **75**, 114008 \(2007\)](#), arXiv:hep-ph/0703172 [hep-ph].
- [23] H. R. Grigoryan, P. M. Hohler, and M. A. Stephanov, [Phys. Rev. D **82**, 026005 \(2010\)](#), arXiv:1003.1138 [hep-ph].
- [24] Y. Li, P. Maris, X. Zhao, and J. P. Vary, [Phys. Lett. B **758**, 118 \(2016\)](#), arXiv:1509.07212 [hep-ph].
- [25] N. R. F. Braga, M. A. Martin Contreras, and S. Diles, [Phys. Lett. B **763**, 203 \(2016\)](#), arXiv:1507.04708 [hep-ph].
- [26] J.-K. Chen, [Phys. Lett. B **786**, 477 \(2018\)](#), arXiv:1807.11003 [hep-ph].
- [27] J.-K. Chen, [Eur. Phys. J. A **57**, 238 \(2021\)](#), arXiv:2102.07993 [hep-ph].
- [28] J.-K. Chen, [Nucl. Phys. A **1050**, 122927 \(2024\)](#), arXiv:2302.05926 [hep-ph].
- [29] M. A. Martin Contreras and A. Vega, [Phys. Rev. D **102**, 046007 \(2020\)](#), arXiv:2004.10286 [hep-ph].
- [30] M. A. Martin Contreras and A. Vega, arXiv preprint (2025), arXiv:2509.04956 [hep-ph].
- [31] S. Navas *et al.* (Particle Data Group), [Phys. Rev. D **110**, 030001 \(2024\)](#).
- [32] N. R. F. Braga, L. F. Ferreira, and R. Da Rocha, [Phys. Lett. B **787**, 16 \(2018\)](#), arXiv:1808.10499 [hep-ph].
- [33] M. A. Martin Contreras and A. Vega, [Phys. Rev. D **108**, 126024 \(2023\)](#), arXiv:2309.02905 [hep-ph].
- [34] A. F. Krutov, R. G. Polezhaev, and V. E. Troitsky, [Phys. Rev. D **93**, 036007 \(2016\)](#), arXiv:1602.00907 [hep-ph].
- [35] T. M. Aliev, A. Ozpineci, and M. Savci, [Phys. Lett. B **678**, 470 \(2009\)](#), arXiv:0902.4627 [hep-ph].
- [36] J. P. Vary *et al.*, [Few Body Syst. **59**, 56 \(2018\)](#), arXiv:1804.07865 [nucl-th].
- [37] M. E. Carrillo-Serrano, W. Bentz, I. C. Cloët, and A. W. Thomas, [Phys. Rev. C **92**, 015212 \(2015\)](#), arXiv:1504.08119 [nucl-th].

- [38] N. Evans and A. Tedder, *Phys. Lett. B* **642**, 546 (2006), arXiv:hep-ph/0609112 [hep-ph].
- [39] S. S. Afonin, *Phys. Rev. C* **83**, 048202 (2011), arXiv:1102.0156 [hep-ph].
- [40] S. S. Afonin, *Int. J. Mod. Phys. A* **27**, 1250171 (2012), arXiv:1207.2644 [hep-ph].
- [41] N. R. F. Braga and L. F. Ferreira, *Phys. Lett. B* **783**, 186 (2018), arXiv:1802.02084 [hep-ph].
- [42] M. A. Martin Contreras and A. Vega, *Phys. Rev. D* **101**, 046009 (2020), arXiv:1910.10922 [hep-th].
- [43] M. A. Martin Contreras, S. Diles, and A. Vega, *Phys. Rev. D* **103**, 086008 (2021), arXiv:2101.06212 [hep-ph].
- [44] M. A. Martin Contreras, A. Vega, and S. Diles, *Phys. Lett. B* **854**, 138723 (2024), arXiv:2308.16007 [hep-ph].
- [45] Y.-G. Ma, L.-G. Pang, R. Wang, and K. Zhou, *Chin. Phys. Lett.* **40**, 122101 (2023), arXiv:2311.07274 [nucl-th].
- [46] K. Zhou, L.-G. Pang, S. Shi, and H. Stoecker, in *Proceedings of Science, FAIRness2022* (2023) p. 064.
- [47] L.-G. Pang, *Int. J. Mod. Phys. E* **33**, 2430009 (2024).
- [48] Z.-H. Li, C.-Q. Li, and L.-G. Pang, (2023), arXiv:2309.07397 [gr-qc].
- [49] K.-F. Pu, H. Li, H.-L. Lu, and L.-G. Pang, *Chin. Phys. C* **47**, 054104 (2023), arXiv:2303.03934 [nucl-th].
- [50] L.-G. Pang, *Nucl. Phys. A* **1005**, 121972 (2021).
- [51] J. Steinheimer, L.-G. Pang, K. Zhou, V. Koch, J. Randrup, and H. Stoecker, *JHEP* **12**, 122 (2019), arXiv:1906.06562 [nucl-th].
- [52] L. Wang, B. M. Hare, K. Zhou, H. Stoecker, and O. Scholten, *Chaos, Solitons & Fractals* **170**, 113346 (2023).
- [53] Y. Huang, J. Chen, J. Jia, L.-M. Liu, Y.-G. Ma, and C. Zhang, (2025), arXiv:2501.01352 [nucl-th].
- [54] W.-B. He, Y.-G. Ma, L.-G. Pang, H. Song, and K. Zhou, *Nucl. Sci. Tech.* **34**, 88 (2023), arXiv:2303.06752 [hep-ph].
- [55] J. He, W.-B. He, Y.-G. Ma, and S. Zhang, *Phys. Rev. C* **104**, 044902 (2021), arXiv:2109.06277 [hep-ph].
- [56] K. Hornik, M. Stinchcombe, and H. White, *Neural Networks* **2**, 359 (1989).

- [57] M. Raissi, P. Perdikaris, and G. E. Karniadakis, *Journal of Computational Physics* **378**, 686 (2019).
- [58] S. Soma, L. Wang, S. Shi, H. Stoecker, and K. Zhou, *Phys. Rev. D* **107**, 083028 (2023), arXiv:2209.08883 [astro-ph.HE].
- [59] G. E. Karniadakis, I. G. Kevrekidis, L. Lu, P. Perdikaris, S. Wang, and L. Yang, *Nature Reviews Physics* **3**, 422 (2021).
- [60] S. Shi, K. Zhou, J. Zhao, S. Mukherjee, and P. Zhuang, *Phys. Rev. D* **105**, 014017 (2022), arXiv:2105.07862 [hep-ph].
- [61] W. He, Q. Li, Y. Ma, Z. Niu, J. Pei, and Y. Zhang, *Sci. China Phys. Mech. Astron.* **66**, 282001 (2023), arXiv:2301.06396 [nucl-th].
- [62] K. Zhou, L.-G. Pang, N. Su, H. Petersen, H. Stoecker, and X.-N. Wang, in *EPJ Web Conf.*, Vol. 171 (2018) p. 16005.
- [63] L.-G. Pang, K. Zhou, N. Su, H. Petersen, H. Stoecker, and X.-N. Wang, *Nucl. Phys. A* **982**, 867 (2019).
- [64] L. Wang, Y. Jiang, L. He, and K. Zhou, *Chin. Phys. Lett.* **39**, 120502 (2022), arXiv:2005.04857 [cond-mat.dis-nn].
- [65] Y.-S. Zhao, L. Wang, K. Zhou, and X.-G. Huang, *Phys. Rev. C* **106**, L051901 (2022), arXiv:2105.13761 [hep-ph].
- [66] Y.-L. Du, D. Pablos, and K. Tywoniuk, *JHEP* **2021**, 206 (2020), arXiv:2012.07797 [hep-ph].
- [67] Y.-L. Du, D. Pablos, and K. Tywoniuk, *Phys. Rev. Lett.* **128**, 012301 (2022), arXiv:2106.11271 [hep-ph].
- [68] L. Jiang, L. Wang, and K. Zhou, *Phys. Rev. D* **103**, 116023 (2021), arXiv:2103.04090 [nucl-th].
- [69] S. Shi, K. Zhou, J. Zhao, S. Mukherjee, and P. Zhuang, in *PoS LATTICE2021* (2022) p. 537.
- [70] H.-A. Zeng, L. Wang, and M. Huang, (2025), arXiv:2512.06044 [hep-lat].
- [71] T. Akutagawa, K. Hashimoto, and T. Sumimoto, *Phys. Rev. D* **102**, 026020 (2020), arXiv:2005.02636 [hep-th].
- [72] K. Hashimoto, S. Sugishita, A. Tanaka, and A. Tomyia, *Phys. Rev. D* **98**, 106014 (2018), arXiv:1809.10536 [hep-th].
- [73] Y.-K. Yan, S.-F. Wu, X.-H. Ge, and Y. Tian, *Phys. Rev. D* **102**, 101902 (2020), arXiv:2004.12112 [hep-th].

- [74] K. Hashimoto, K. Ohashi, and T. Sumimoto, *Phys. Rev. D* **105**, 106008 (2022), arXiv:2108.08091 [hep-th].
- [75] M. Song, M.-S. H. Oh, Y. Ahn, and K.-Y. Kim, *Chin. Phys. C* **45**, 073111 (2021), arXiv:2011.13726 [physics.class-ph].
- [76] W.-B. Chang and D.-f. Hou, *Phys. Rev. D* **109**, 086010 (2024), arXiv:2403.04966 [hep-ph].
- [77] B. Ahn, H.-S. Jeong, K.-Y. Kim, and K. Yun, *JHEP* **2024**, 141 (2024), arXiv:2401.00939 [hep-th].
- [78] Z.-F. Gu, Y.-K. Yan, and S.-F. Wu, (2024), arXiv:2401.09946 [hep-th].
- [79] K. Li, Y. Ling, P. Liu, and M.-H. Wu, *Phys. Rev. D* **107**, 066021 (2023), arXiv:2209.05203 [hep-th].
- [80] R.-G. Cai, S. He, L. Li, and H.-A. Zeng, (2024), arXiv:2406.12772 [hep-th].
- [81] B. Ahn, H.-S. Jeong, K.-Y. Kim, and K. Yun, (2024), arXiv:2406.07395 [hep-th].
- [82] H. Boschi-Filho and N. R. F. Braga, *JHEP* **05**, 009 (2003), arXiv:hep-th/0212207.
- [83] B. Batell and T. Gherghetta, *Phys. Rev. D* **78**, 026002 (2008), arXiv:0801.4383 [hep-ph].
- [84] W. Lucha and F. F. Schoberl, *Phys. Rev. A* **54**, 3790 (1996), arXiv:hep-ph/9603429.
- [85] J. Polchinski and M. J. Strassler, *JHEP* **05**, 012 (2003), arXiv:hep-th/0209211.
- [86] M. B. Wise, in *Les Houches Summer School in Theoretical Physics, Session 68: Probing the Standard Model of Particle Interactions* (1997) pp. 1051–1089, arXiv:hep-ph/9805468.
- [87] S. S. Afonin, *PMC Phys. A* **3**, 1 (2009), arXiv:0710.4921 [hep-ph].
- [88] S. S. Afonin, A. A. Andrianov, V. A. Andrianov, and D. Espriu, *JHEP* **04**, 039 (2004), arXiv:hep-ph/0403268.
- [89] W. Lucha, F. F. Schoberl, and D. Gromes, *Phys. Rept.* **200**, 127 (1991).
- [90] M. A. M. Contreras, S. Diles, and A. Vega, arXiv preprint arXiv:2101.06212 (2021), arXiv:2101.06212 [hep-ph].
- [91] S. Navas *et al.* (Particle Data Group), *Phys. Rev. D* **110**, 030001 (2024).